Eur Biophys J (2012) 41:41–51
DOI 10.1007/s00249-011-0756-6

ORIGINAL PAPER

EBSA
Biophysics in Europe

# Folding of an all-helical Greek-key protein monitored by quenched-flow hydrogen–deuterium exchange and NMR spectroscopy

**Lesley H. Greene · Hai Li · Junyan Zhong · Guoxia Zhao · Khym Wilson**

Received: 7 July 2011 / Revised: 21 September 2011 / Accepted: 2 October 2011 / Published online: 1 December 2011


**Abstract** To advance our understanding of the protein folding process, we use stopped-flow far-ultraviolet (far-UV) circular dichroism and quenched-flow hydrogen–deuterium exchange coupled with nuclear magnetic resonance (NMR) spectroscopy to monitor the formation of hydrogen-bonded secondary structure in the C-terminal domain of the Fas-associated death domain (Fadd-DD). The death domain superfamily fold consists of six $\alpha$-helices arranged in a Greek-key topology, which is shared by the all-$\beta$-sheet immunoglobulin and mixed $\alpha/\beta$-plait superfamilies. Fadd-DD is selected as our model death domain protein system because the structure of this protein has been solved by NMR spectroscopy, and both thermodynamic and kinetic analysis indicate it to be a stable, monomeric protein with a rapidly formed hydrophobic core. Stopped-flow far-UV circular dichroism spectroscopy revealed that the folding process was monophasic and the rate is 23.4 $s^{-1}$. Twenty-two amide hydrogens in the backbone of the helices and two in the backbone of the loops were monitored, and the folding of all six helices was determined to be monophasic with rate constants between 19 and 22 $s^{-1}$. These results indicate that the formation of secondary structure is largely cooperative and concomitant with the hydrophobic collapse. This study also provides unprecedented insight into the formation of secondary structure within the highly populated Greek-key fold more generally. Additional insights are gained by calculating the exchange rates of 23 residues from equilibrium hydrogen–deuterium exchange experiments. The majority of protected amide protons are found on helices 2, 4, and 5, which make up core structural elements of the Greek-key topology.

**Keywords** Fas-associated death domain · Greek-key topology · Deuterium–hydrogen exchange · NMR spectroscopy · Protein folding · Quenched flow

**Abbreviations**

| | |
|---|---|
| Fadd-DD | C-terminal domain of the Fas-associated death domain |
| CARD | Caspase recruitment domain |
| CD | Circular dichroism |
| HSQC | Heteronuclear single quantum coherence |
| DTT | Dithiothreitol |
| HX | Hydrogen–deuterium exchange |
| GndHCl | Guanidine hydrochloride |
| MES | 2-(*N*-morpholino) ethanesulfonic acid |
| NMR | Nuclear magnetic resonance |
| UV | Ultraviolet |

L. H. Greene and H. Li contributed equally.

**Electronic supplementary material** The online version of this article (doi:10.1007/s00249-011-0756-6) contains supplementary material, which is available to authorized users.

L. H. Greene (✉) · H. Li · G. Zhao · K. Wilson
Department of Chemistry and Biochemistry,
Old Dominion University, 4541 Hampton Boulevard,
Norfolk, VA 23529, USA
e-mail: lgreene@odu.edu

*Present Address:*
H. Li
Department of Biochemistry, Baylor College of Medicine,
Houston, TX 77030, USA

J. Zhong
College of Sciences Major Instrumentation Cluster,
Old Dominion University, 4402 Elkhorn Avenue,
Norfolk, VA 23529, USA

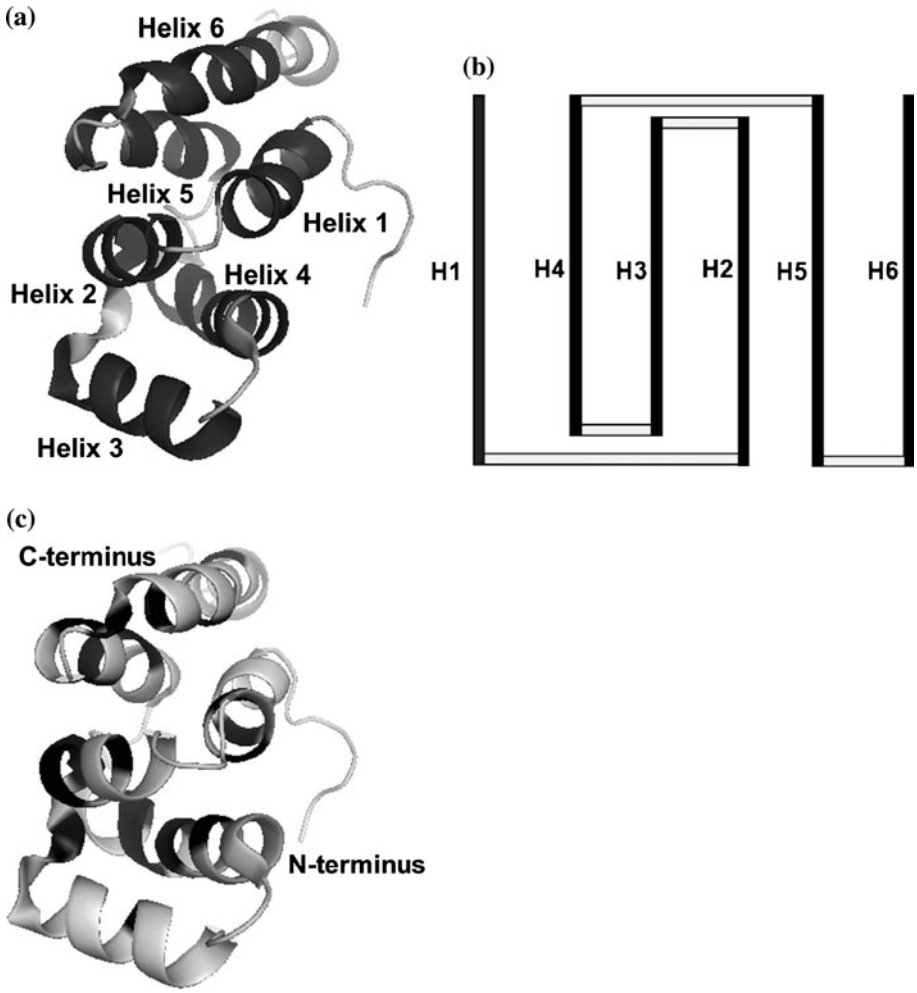


**Fig. 1** Structure of Fadd-DD (PDB code: 1e3y). **a** Ribbon diagram of Fadd-DD drawn in PyMOL v0.99 (DeLano Scientific). The six helices are annotated. The canonical core elements of the Greek-key topology are helices 1, 2, 4, and 5. **b** Schematic of the Greek key. The six helices are denoted H1–H6 in *black* and loops in *gray*. **c** Location of the 23 backbone amides which persist for over 24 h and thus are the most stable in Fadd-DD (F101, V103, C105, L115, R117, Q118, L119, V121, I129, V141, S144, L145, I147, W148, K149, V162, G163, A164, R166, M170, A174, V177, and Q182) are shown in *black* in the context of the secondary and tertiary structure using PyMOL

## Introduction

The protein folding problem remains one of the most challenging and fascinating questions in science today. Advances have been made through computational and experimental study of representative proteins from across fold space. This has led to the development of models that establish a conceptual framework to explain common and unique features in the folding of proteins. The Greek-key topology is one of the most prevalent in nature (Greene et al. 2007). However, at present, there is a lack of detailed information on the formation of secondary structure, which is essential to develop and refine models for this highly populated fold. Interestingly, members of the all-$\alpha$-helical death domain superfamily, the all-$\beta$-sheet immunoglobulin superfamily, and the mixed $\alpha/\beta$-plait superfamily share this common topology, although they differ in secondary structure composition (Higman and Greene 2006). In this report we present results of a folding study using atomic-level resolution for the C-terminal domain of the Fas-associated death domain. More specifically, we monitor the formation of hydrogen-bonded secondary structure in our model system. The death domain superfamily comprises four families: death domain (DD), death effector domain, caspase recruitment domain (CARD), and pyrin domain (Park et al. 2007). They function in either intracellular signal transduction of apoptosis or innate inflammation (Park et al. 2007). The Fas-associated death domain consists of an N-terminal death effector domain and a C-terminal death domain (Fadd-DD) composed of 100 residues and 6 $\alpha$-helices (Berglund et al. 2000; Carrington et al. 2006). Fadd-DD is selected as our model death domain protein system because its NMR structure has been solved, the protein is monomeric, and the kinetic behavior has been characterized by stopped-flow fluorescence spectroscopy (Berglund et al. 2000; Li et al. 2009; Steward et al. 2009). Figure 1a, b shows the six $\alpha$-helices arranged in a Greek-key topology in Fadd-DD (Higman and Greene 2006; Steward et al. 2009).

A combination of quenched-flow methods, hydrogen–deuterium exchange (HX), and nuclear magnetic resonance (NMR) spectroscopy can give detailed site-specific information about the protein folding process by monitoring the formation of individual hydrogen bonds (Englander and

Mayne 1992; Dyson and Wright 1996; Krishna et al. 2004). Quenched-flow HX studies of the folding of a number of proteins have been reported, such as ribonuclease A, cytochrome c, T4 lysozyme, bacteriophage $\lambda$ lysozyme, hen egg white lysozyme, ribonuclease $T_1$, staphylococcal nuclease, immunoglobulin binding domain of streptococcal protein G, apomyoglobin, dihydrofolate reductase, acyl-CoA binding protein, human fibroblast growth factor, hisactophilin, cobrotoxin, and onconase (Roder et al. 1988; Udgaonkar and Baldwin 1988; Lu and Dahlquist 1992; Radford et al. 1992; Mullins et al. 1993; Jacobs and Fox 1994; Jones and Matthews 1995; Garcia et al. 2000; Teilum et al. 2000; Samuel et al. 2001; Liu et al. 2002; Bai 2006; Hsieh et al. 2006; Schulenburg et al. 2009; Di Paolo et al. 2010). The results of several of these studies show that certain parts of a protein may fold earlier than other regions (Radford et al. 1992; Samuel et al. 2001; Schulenburg et al. 2009). However, in other proteins such as phage $\lambda$ lysozyme and the immunoglobulin binding domain of streptococcal protein G the kinetics of secondary structure formation indicates that they form cooperatively (Kuszewski et al. 1994; Di Paolo et al. 2010). We are interested in determining if the helices which make up the canonical Greek-key structure (helices 1, 2, 4, 5) form on a faster folding timescale than the other helices (3 and 6) as well as their order of formation in order to develop a detailed model of folding for Fadd-DD (Fig. 1a, b). Quenched-flow hydrogen–deuterium exchange can address this question by specifically monitoring the formation of hydrogen bonds in each helix during the folding process.

Within the death domain superfamily, the folding behavior of three members of the caspase recruitment domain (CARD) family have been previously studied by stopped-flow techniques. These are caspase recruitment domain of the RIP-like interacting CLARP kinase (RICK-CARD), caspase recruitment domain of apoptotic protease activating factor 1 (Apaf-1-CARD), and procaspase-1, which show complex kinetics. The refolding of RICK-CARD contains multiple phases as well as kinetically trapped species (Chen and Clark 2003; Chen and Clark 2006). Apaf-1-CARD appears to fold via parallel paths due to two unfolded conformations (Milam et al. 2007; Rao et al. 2009), while procaspase-1, like RICK-CARD, also folds through kinetically trapped species (Chen and Clark 2004). In comparison, the folding pathway of Fadd-DD appears to be more straightforward and is thus a good model in which to investigate the determinants of the all-$\alpha$-helical Greek-key topology. Thermodynamic studies of Fadd-DD have been conducted previously (Li et al. 2009; Steward et al. 2009). Fadd-DD is stable and undergoes a reversible and cooperative two-state unfolding/refolding transition. Stopped-flow fluorescence studies by our group indicate that folding is biphasic with the majority of the process occurring in the first phase (Li et al. 2009).

In our present experiments using stopped-flow far-UV circular dichroism (CD), the folding of the secondary structure of Fadd-DD was determined to be monophasic with a rate constant of 23.4 $s^{-1}$. In a more detailed study using a combination of quenched-flow HX and NMR spectroscopy the folding of 22 amide hydrogens in the backbone of the 6 helices and 2 amide hydrogens in the backbone of loops are monitored. The results indicate that the folding of all six helices is monophasic with rate constants calculated between 19 and 22 $s^{-1}$. These data indicate that the formation of hydrogen-bonded secondary structure is fundamentally cooperative. In addition, the equilibrium HX of Fadd-DD was also performed and the exchange rates of 23 residues calculated. Most of the amide protons which are slowest to exchange are in the core region. In summary, this provides the earliest analysis of folding kinetics monitored by quenched-flow and NMR spectroscopy conducted on a protein with a Greek-key topology, although a folding intermediate was studied by amide hydrogen exchange using a pH competition method and rapid mixing with the immunoglobulin CD2 (Parker et al. 1997).

## Materials and methods

### Materials

$^{15}$N-labeled ammonium chloride and 99.0% deuterium oxide were purchased from Cambridge Isotope. High-purity 8 M GndHCl stock solution was purchased from Pierce. 2-(*N*-morpholino) ethanesulfonic acid (MES), glycine, and citric acid were purchased from Fisher. Dipotassium phosphate and dithiothreitol (DTT) were purchased from VWR. All other chemicals were of reagent grade. Deuterated guanidine hydrochloride (GndHCl), DTT, citric acid, and $K_2HPO_4$ were prepared by dissolving the chemicals into $D_2O$ and lyophilizing. This procedure was repeated three times. The concentration of GndHCl used in the experiments was determined with an Atago handheld refractometer (Japan).

### Protein labeling, expression, and purification

Recombinant human Fadd-DD (11.8 kD) uniformly labeled with $^{15}$N was purified from a 6 l fermentation of *Escherichia coli* BL21(DE3) (Novagen) (Li et al. 2009). The cells were grown at 37°C on M9 minimal medium supplemented with 1 g/l $^{15}NH_4Cl$, 0.2 mg/ml carbenicillin, 0.1 mM $CaCl_2$, 2 mM $MgSO_4$, 4 g/l glucose, and 1 ml/l poly-Vi-Sol vitamin drops with iron. The protein has four

amino acids on the N-terminus left from the cloning site. The yield was approximately 15 mg/l. The protein was lyophilized in preparation for denaturation and refolding in the quenched-flow studies. Unlabeled protein for the stopped-flow far-UV CD studies was expressed and purified according to previously established protocols by the authors (Li et al. 2009).

### Quenched-flow experiments

The preparation of the samples for the HX methods utilized a Bio-Logic SFM-400 (France) and the following Bio-Logic delay lines: N°1 (17), N°3 (90), and N°5 (190) at 20°C. $^{15}$N-Fadd-DD (1 mg/ml) was denatured in 5 M deuterated GndHCl, 10 mM deuterated MES (pD 6.2), and 5 mM deuterated DTT overnight. The pD of the deuterated buffer solution was determined by adding 0.4 units to the reading of the pH probe (Primrose 1993). Refolding was initiated by mixing one volume of the denatured protein solution with four volumes of water-based refolding buffer containing 10 mM MES (pH 6.2) and 5 mM DTT. The concentrations of GndHCl and protein at this point are 1 M and 0.2 mg/ml, respectively. Under this concentration, the protein was shown to be in the native state and the folding of the protein is not concentration dependent (Li et al. 2009). After refolding for a specified period of time, the protein was mixed with five volumes of water-based pulsing buffer containing 50 mM glycine buffer (pH 9.8) and 5 mM DTT, thus being subjected to a high pH pulse step for 5.4 ms. This induces the amide deuterium on the protein to exchange with hydrogen in the solvent. The first three refolding times (9.9, 28.1, and 53.2 ms) were used under continuous mode, and the last five (65, 80, 120, 160, and 200 ms) were used under interrupted mode. Continuous mode means that the mixed reactants are continuously pushed through the delay line at a steady and calculated rate. At the end of the delay line, the reactants have been aged for the required time. In interrupted mode the pushing phase is interrupted to allow for user-controlled aging. When the aging time has been reached the solution is pushed out of the delay line. The protein sample was then allowed to continue refolding at a lower pH followed by mixing with ten volumes of water-based quenching buffer containing 200 mM $K_2HPO_4$/100 mM citric acid (pH 3.9) and 5 mM DTT. The final pulse and quench pH after dilution were 9.8 and 4.7, respectively. The average intrinsic exchange relaxation times from amide deuterium to amide hydrogen in $H_2O$ at 20°C are approximately 1.7 s, 0.4 ms, and 44 s for the refolding, pulse, and quench steps, respectively (http://hx2.med.upenn.edu/download.html). Therefore, the hydrogen labeling only occurs when the protein was mixing with pulsing buffer. To prepare the samples for NMR studies the solutions were concentrated using Vivaspin 20 concentrators (Sartorius Stedim) at 7,500 rpm at 4°C for approximately 12 h immediately following the quenched-flow experiments and stored overnight at 4°C. The next day, the buffer of the solution was exchanged into 100 mM deuterated $K_2HPO_4$/50 mM deuterated citric acid (pD 4.8) and 10 mM deuterated DTT in $D_2O$ for approximately 12 h at 4°C, to exchange the amide hydrogens with no or weak hydrogen-bond protection, and then immediately used for NMR. pD 4.8 was selected because the number of stable amide protons was maximal in comparison with those at pD 7.6, 6.2, and 5.2.

### NMR studies

The NMR experiments were conducted on a Bruker AVANCE III 400-MHz NMR spectrometer in the College of Sciences Major Instrumentation Cluster, Old Dominion University. All NMR spectra (1D and 2D) were collected at 30°C. The acquisition time for 2D NMR is approximately 5.5 h. To obtain residue-specific information about the refolding of Fadd-DD from the HX experiments, the backbone peaks of $^{1}$H-$^{15}$N heteronuclear single quantum coherence (HSQC) spectra for the native Fadd-DD were obtained and compared with the literature (Berglund et al. 2000). Sensitivity-enhanced $^{1}$H-$^{15}$N HSQC spectra were obtained on a 5-mm inverse conventional probe with globally optimized alternating phase rectangular pulse (GARP) decoupling in the $^{15}$N channel. Along the F2 dimension, 1,024 complex points were collected, and 128 transients were accumulated along the F1 dimension. $^{15}$N chemical shifts were referenced indirectly using the consensus chemical shift ratio of 0.101329118. All the HSQC spectra were generated in NMRPipe by apodizing the free induction decay (FID) with a cosine window, followed by zero-filling to the next power of 2, Fourier transformation, and phasing in both F1 and F2 dimension, and visualized with NMRDraw (Delaglio et al. 1995). In the native HSQC spectra two pairs of peaks are difficult to assign due to overlap. These are I147 and L172 as well as V177 and D185. However, we calculated with the program Contact (Winn et al. 2011) that D185 and L172 do not form main-chain hydrogen bonds in the native state. Therefore, in $D_2O$ these peaks will not be present. Thus, the resonance assignments of I147 and V177 were deconvoluted and used in our present studies.

### Data analysis

Hydrogen bonds were calculated using the program Contact (Winn et al. 2011) and further confirmed with Insight II (Accelrys). The HSQC peak intensities from the quenched-flow studies were normalized to a control experiment. In the control experiment, water-based buffers

were used in the unfolding and refolding portions of the quenched-flow experiment. The protein was then concentrated and buffer exchanged as specified earlier. One-dimensional proton NMR spectra were used to calibrate the concentration difference among protein samples from different time points in TopSpin software (Bruker) (Nabuurs and van Mierlo 2010). The absolute peak intensity of the well-resolved resonance at -0.37 ppm, which corresponds to a nonexchangeable methyl proton resonance from L119, is a direct measure of the protein concentration in the corresponding NMR sample. The HSQC peak intensities were normalized using the absolute peak intensities of the upfield resonances in the 1D spectra to correct the small variation of protein concentration in the samples. The resultant data were plotted using SigmaPlot, version 10 (Systat Software), and kinetic rates determined by applying the single exponential equation to 24 peaks monitored during the study were analyzed. The peak intensities were calculated with NMRDraw.

### Equilibrium hydrogen exchange

In the equilibrium HX study, $^{15}$N-Fadd-DD (4 mg/ml) was buffer exchanged into 100 mM deuterated $K_2HPO_4$/50 mM deuterated citric acid and 5 mM deuterated DTT in 99.0% $D_2O$ (pD 4.8). Each HSQC spectrum was acquired every 8 h over the course of 1 week. HX rates were determined by fitting peak intensities from HSQC spectra as a function of time using a single exponential equation in SigmaPlot. The intensities of each identified peak are normalized against that in the first HSQC spectrum. The protection against exchange rate is expressed as the protection factor, which is the ratio between the sequence-specific intrinsic exchange rate for an amide proton $k_{int}$, and measured exchange rate $k_{ex}$ (Bai et al. 1993; Sasakawa et al. 1999). $k_{int}$ was calculated using an intrinsic exchange rate program (H in $D_2O$) located at http://hx2.med.upenn.edu/download.html. The protection factors are calculated for the slowly exchanging peaks. The time-zero resonance peak for V177 is not considered in the analysis because it is lower than the intensity at 8 h and prohibits calculation of an accurate kinetic rate. However, the peak volume decreases as expected, so this phenomenon is not understood.

### Secondary structure formation studied with stopped-flow far-UV CD

The kinetics of refolding of Fadd-DD was measured at 20°C on a Bio-Logic MOS 450 stopped-flow instrument using far-UV CD detection. Protein (0.9 mg/ml) was unfolded in 20 mM MES (pH 6.2), 5 mM DTT, and 6 M GndHCl. Refolding experiments were carried out by rapid 1:5 dilution of the protein solution in 20 mM MES (pH 6.2) at 20°C, giving final concentrations of protein and GndHCl of 0.15 mg/ml and 1 M, respectively. The dead time was 9.3 ms. Change in the far-UV CD signal was monitored in an FC-20 cuvette (2 mm path length) at 225 nm. The excitation and emission slits were both 2 mm. The refolding experiments were repeated 20 times, and the averaged traces were fitted to a single exponential equation in SigmaPlot. The denatured baseline was obtained by mixing the denatured protein with denaturing buffer in the stopped-flow system and measuring the CD signal at 225 nm. The native baseline was determined by mixing native protein with refolding buffer in the stopped-flow system and measuring the CD signal at 225 nm. Both baselines were calculated from an average of 20 shots each.

## Results

### Equilibrium HX studies

The HX rate is dependent on the conditions such as pH and temperature (Englander and Mayne 1992). The rates of HX ($k_{ex}$) of slowly exchanged amide protons of native Fadd-DD were measured at pD 4.8 and 30°C by recording HSQC spectra every 8 h for 1 week. Exchange of three amide protons was observed at this pH but was too fast to be measured. Except for some overlapping peaks in the spectra, a large number of backbone amide protons are exchanged during the process of buffer exchange. Thus, exchange rates of 23 slowly exchanging amide protons which are defined as those that persist for 24 h or more in Fadd-DD during the NMR acquisition time were calculated. Normalized intensities of eight peaks with the slowest exchange rates are shown as a function of time in Fig. 2a. Protected amides occur in all six helices (Figs. 1c, 2b). However, the majority of protected amide protons are found on helices 2, 4, and 5. Most assigned peaks are not visible after 1 week, except for four: I147, W148, V162, and V177. The persistent hydrogen bonds between S144-I147, S144-W148, V158-V162, and V173-V177 suggest that these regions within helices 4, 5, and 6 are very stable. The native HSQC spectrum of Fadd-DD in $K_2HPO_4$/citric acid buffer (pH 4.8) and 10% $D_2O$ is shown in Supplementary Fig. S1 and is similar to the previously published HSQC in potassium phosphate buffer (pH 6.2) (Berglund et al. 2000).

### Stopped-flow far-UV CD spectroscopy

The folding kinetics of Fadd-DD monitored by far-UV CD revealed the rate of secondary structure formation (Fig. 3). One single phase with rate constant of 23.4 ± 0.4 $s^{-1}$ and

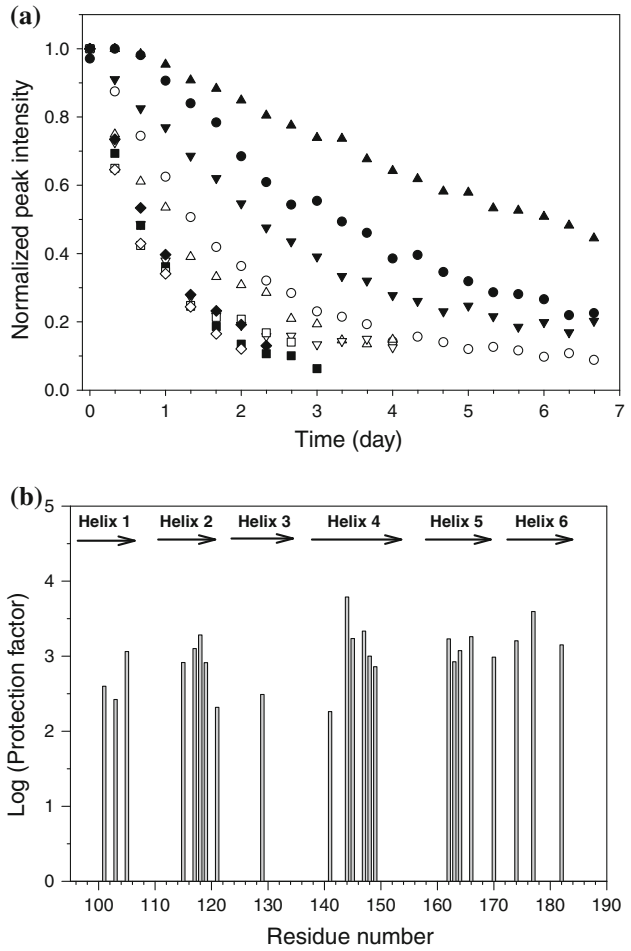


**Fig. 2** Equilibrium amide hydrogen exchange in Fadd-DD. **a** The HX of the 10 slowest exchanging peaks: L115 (*white diamonds*), L119 (*white down triangles*), S144 (*white squares*), L145 (*white up triangles*), I147 (*black down triangles*), W148 (*white circles*), V162 (*black circles*), R166 (*black diamonds*), A174 (*black squares*), and V177 (*black up triangles*) are plotted. **b** Histogram showing the distribution of protection factors for the native protein at pD 4.8 and 30°C versus residue number. Regions of secondary structure are indicated schematically

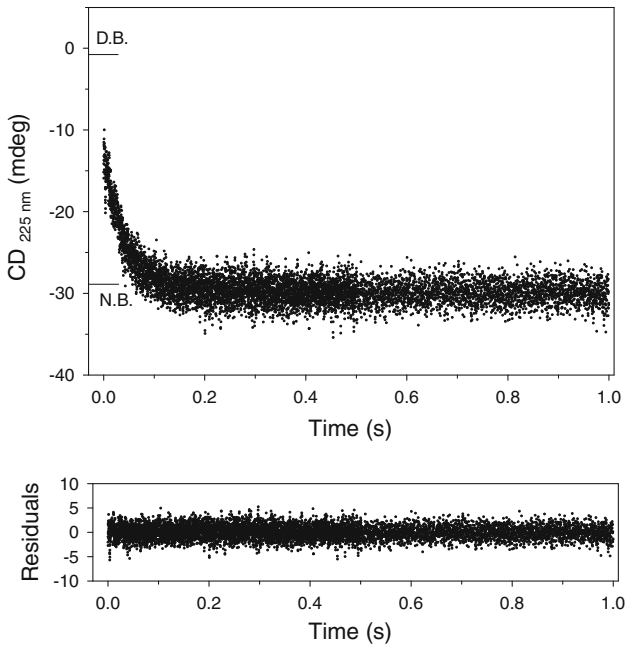


**Fig. 3** Stopped-flow circular dichroism study of Fadd-DD. The folding process was initiated with a 1:5 dilution at 20°C. Refolding of denatured WT protein at 0.15 mg/ml in 20 mM MES buffer (pH 6.2) and 5 mM DTT was monitored by stopped-flow far-UV CD spectroscopy at 225 nm. The dead time was 9.3 ms. The timescale of formation of secondary structure is 43 ms. The residuals are shown below the time course. D.B. and N.B. are denatured state and native state baselines, respectively

amplitude of $16.8 \pm 0.1$ millidegrees was calculated (Table 1). Based on the signal intensity of the denatured state baseline and the starting location of the refolding trace there appears to be a burst phase in the 9.3 ms dead time of the instrument (Nölting 2006).

## Hydrogen exchange and quenched flow coupled with NMR spectroscopy

Following HX into $D_2O$ buffer, a total of 24 well-resolved and assignable amide protons were identified to be stable. Protected amides were found in all six α-helices. However, the number of protected amides did not distribute evenly among the six helices; for example, only one amide proton (I129) in helix 3 was protected. The hydrogen-bonding pattern in Fadd-DD is shown in Fig. 4. The amide protons of N107 and R140 have very high exchange rates, and the peaks disappear after 16 h of exchange. They are therefore not counted among the 24 stable amide protons to be used in quenched-flow kinetic studies.

The ratio of volume among the protein solution, refolding buffer, and pulse buffer was 1:4:5. The content of proton and deuterium after mixing of the three buffers were 90% and 10%, respectively. Therefore, the maximum proton occupancy of the quenched-flow study was 90%.

The structural details of the folding reaction were obtained by analyzing the samples by 2D $^{1}H$-$^{15}N$ HSQC measurements. HSQC spectra are shown in Fig. 5. A total of 22 amide protons could be monitored in the 6 helices. Fig. 6 displays the protection time courses obtained for individual amides, grouped according to their distribution in different helices. All of the kinetics were found to be monophasic, and a single exponential function could be used to fit the data satisfactorily (Fig. 6). In addition, two amide protons from two residues (V121 and M170) located in loop structures could also be monitored with kinetic rate constants of $20.7 \pm 7.0\ s^{-1}$ and $21.3 \pm 6.7\ s^{-1}$, respectively (Fig. 6). The resulting curves are very similar, with rate constants between 19 and 22 $s^{-1}$ (Table 1). The

**Table 1** Rate Constants of hydrogen-bond formation within each helix of Fadd-DD

| | Rate ($s^{-1}$) | Amplitude |
|---|---|---|
| Secondary structure formation (stopped-flow far-UV CD) | 23.4 ± 0.3 | 16.8 ± 0.1 |
| Average hydrogen-bond formation (quenched-flow/NMR spectroscopy) | 20.9 ± 1.7 | 0.7 ± 0.0 |
| Helix 1 | 19.1 ± 4.0 | 0.8 ± 0.1 |
| Helix 2 | 21.0 ± 3.4 | 0.7 ± 0.0 |
| Helix 3 | 19.7 ± 7.0 | 0.7 ± 0.1 |
| Helix 4 | 21.0 ± 3.0 | 0.8 ± 0.0 |
| Helix 5 | 22.5 ± 4.2 | 0.7 ± 0.1 |
| Helix 6 | 20.9 ± 5.4 | 0.7 ± 0.1 |

average rate constant of hydrogen-bond formation is 20.9 ± 1.7 $s^{-1}$ (Table 1). The results indicate that all detectable amides acquire protection from exchange concomitantly, with simple mono-exponential time courses. No intermediate, partially protected species are observable in these experiments, and folding appears to be highly cooperative.

## Discussion

In the equilibrium HX study conducted by Jeong et al. with mouse Fadd-DD, 35 residues spanning the 6 helices were shown to have the slowest exchanging protons in an equilibrium HX study (Jeong et al. 1999). Invariably, residues involved in the hydrophobic core have the slowly exchanging protons. Among these 35 residues, 21 residues are strongly protected in the human Fadd-DD as well. The backbone amides with hydrogen bonds in the loops of both mouse and human Fadd-DD, V121 and L170 (M170 in human homolog), are protected. More backbone amides from mouse Fadd-DD were found to have slower exchange rates than human Fadd-DD. However, it may be explained that, in our study, the protein goes through approximately 12 h of buffer exchange from the water-based buffer to $D_2O$-based buffer due to the existence of three free cysteines, which prevents the protein from being lyophilized for the equilibrium HX experiment. Thus, some of the backbone residues with weak hydrogen bonds may be exchanged during the process, whereas the mouse Fadd-DD was lyophilized and directly dissolved in $D_2O$. The pH also differed; with mouse Fadd-DD, pH 4.0 was used.

For human Fadd-DD, only one slowly exchanging amide group was found in helix 3 in comparison with the other helices. This observation is in good agreement with the discovery that helix 3 is more mobile than the other helices (Berglund et al. 2000). The lack of substantial protection could suggest that this helix is less stable. However, the fact that helix 3 has higher relative solvent accessibility than the other helices shows that this helix is clearly more exposed and may account for limited

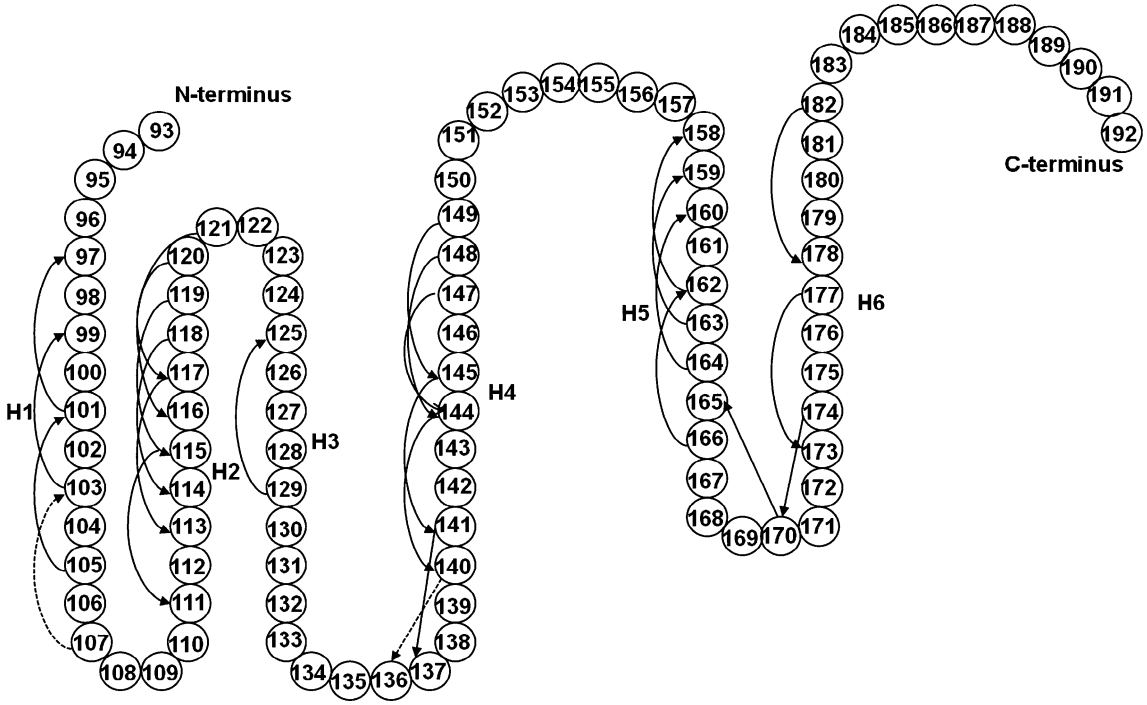


**Fig. 4** Hydrogen-bonding pattern of Fadd-DD. *Curves* and *arrows* indicate the hydrogen bonding and the direction. *Dashed lines* show the two unstable hydrogen bonds of N107 and R140

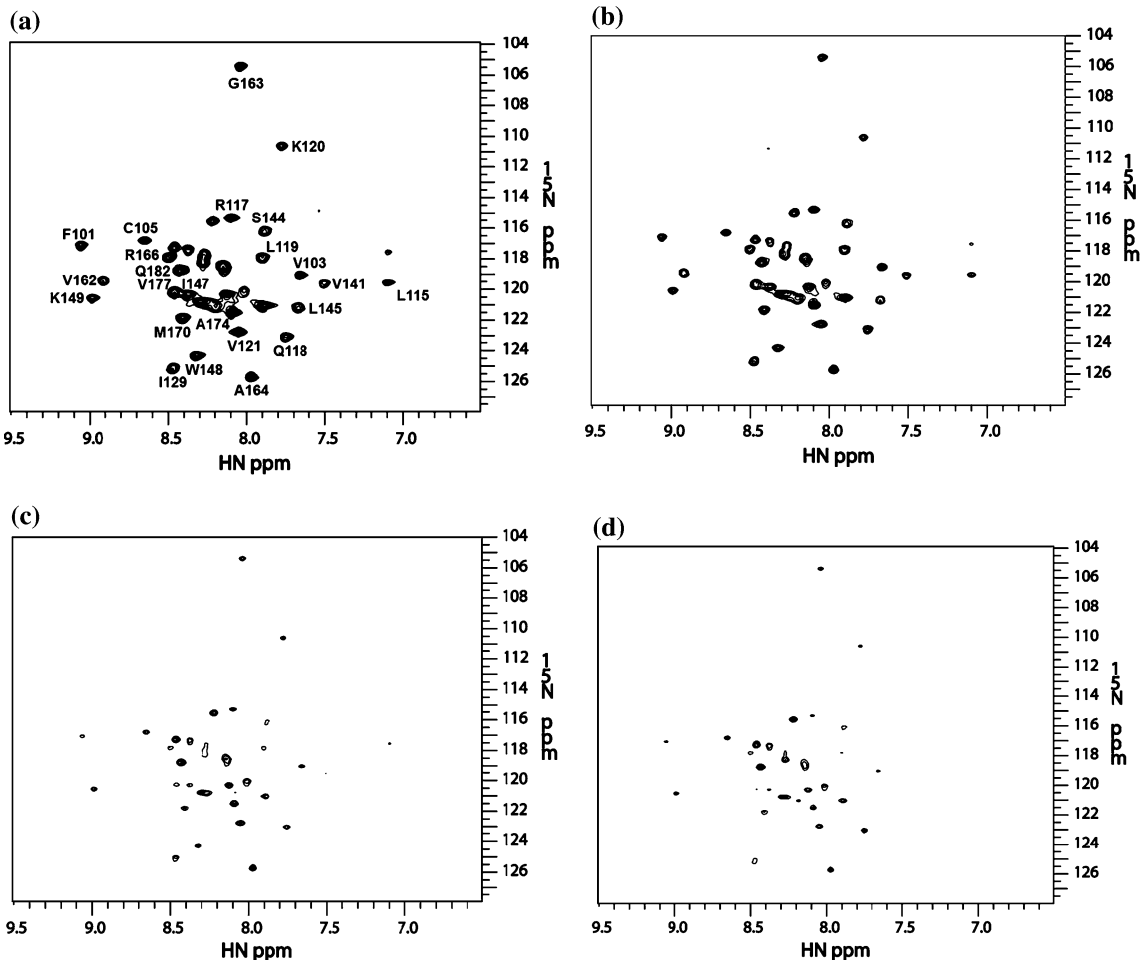


**Fig. 5** HSQC spectra of 4 mg/ml Fadd-DD in $D_2O$ after quenched-flow folding and buffer exchange into $D_2O$ buffer (100 mM $K_2HPO_4$/ 50 mM citric acid, pD 4.8). Select refolding times are shown in the following panels: **a** 9.9 ms, **b** 53.2 ms, **c** 80 ms, and **d** 200 ms. The hydrogen-bond formation of 24 residues (22 in the helices and 2 in the loops) are followed

protection (Berglund et al. 2000). In mouse Fadd-DD, helix 3 also has the most internal flexibility of all helical elements according to the profile of amide solvent exchange rates (Jeong et al. 1999).

There appears to be only a limited number of equilibrium HX studies conducted on proteins with the Greek-key topology. While they can have different secondary structure it is interesting to compare and contrast the proteins investigated, though speculatively. In one study on ribosomal S6, which belongs to the $\alpha/\beta$-plait superfamily, the amide protons located in $\beta1$, $\alpha1$, and $\beta3$ had greater protection factors (Haglund et al. 2009). They correspond with protected helices 1, 2, and 4 in Fadd-DD, respectively (Higman and Greene 2006). Llama antibody fragment, which belongs to the all-$\beta$ immunoglobulin superfamily, has more complex secondary elements consisting of 11 $\beta$-strands. However, it appears that strands 4 and 9, which correspond to protected helices 2 and 5 in Fadd-DD, have the highest protection factors (Higman and Greene, 2006; Pérez et al. 2001). Thus, in both representatives, there is significant protection in elements of the canonical core of the Greek-key form (Fig. 1). Mutations applied in Fadd-DD by our group previously showed that even a conservative change to W148 significantly destabilizes the native state (Li et al. 2009). Interestingly, this residue in involved in one of the most persistent hydrogen bonds (Figs. 1c, 2a).

There is good agreement between folding rates measured by stopped-flow far-UV CD and quenched flow, indicating that they monitor the same cooperative transition, also being similar to the first and dominant phase of folding monitored by stopped-flow fluorescence spectroscopy (22.7 $s^{-1}$) (Li et al. 2009). While there is only one phase indicated by stopped-flow far-UV CD and quenched-flow and two phases for the study of stopped-flow fluorescence, this is not an unprecedented result. There are examples of several proteins which also show similar kinetic behavior; for example, the study conducted on bacteriophage $\lambda$ lysozyme showed that there are two phases for intrinsic fluorescence and far-UV CD, but only one phase for both HX and NMR as well as HX and mass

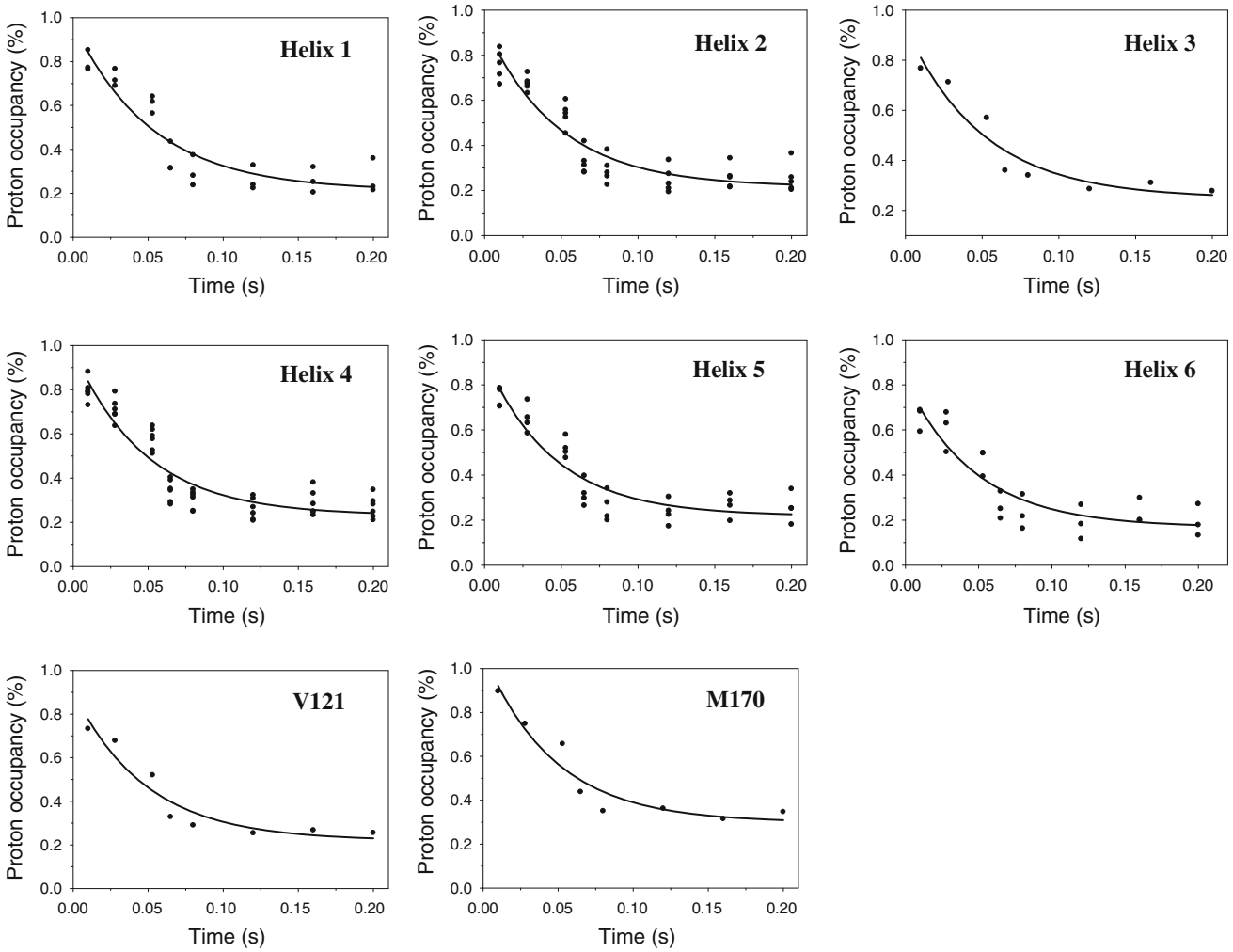


**Fig. 6** Kinetics of hydrogen-bond formation of 22 residues in the 6 helices and 2 in the loops of Fadd-DD. The eight panels show the proton occupancies of backbone amides from helix 1 (F101, V103, and C105), helix 2 (L115, R117, Q118, L119, and K120), helix 3 (I129), helix 4 (V141, S144, L145, I147, W148, and K149), helix 5 (V162, G163, A164, and R166), and helix 6 (A174, V177, and Q182) as well as the kinetics of hydrogen-bond formation of two loop residues V121 and M170. These data were fitted to a single exponential equation to calculate the folding rate using SigmaPlot. The average timescale of hydrogen-bond formation in the helices is 48 ms

spectrometry (Di Paolo et al. 2010). Additionally, for human fibroblast growth factor, two phases were detected for stopped-flow fluorescence spectroscopy, one phase for stopped-flow far-UV CD, and multiple rates for HX and NMR (Samuel et al. 2001).

In the quenched-flow experiment conducted on phage $\lambda$ lysozyme, it was suspected that two factors account for the 15–20% lack of protection: (1) some back-exchange of deuterium for hydrogen occurred following quenching and before the final buffer exchange into the $D_2O$ buffer; (2) sample preparation required several hours due to the large amount of protein needed for NMR (Di Paolo et al. 2010). We think that these factors also apply to our experiment, which could explain the fact that proton occupancy of all amides does not go to approximately zero. It should be noted that in our study the data were plotted with peak intensity because the standard errors are less than when plotted with peak volume, although the time scales of hydrogen-bond formation are similar.

## Conclusions

The folding behavior of individual amide protons with HX quenched-flow and NMR spectroscopy has been monitored on well over 10 proteins. In some proteins, it is shown that select amide protons on specific structural features fold earlier than the others. For example, in $\beta$-lactoglobulin, it was found that, during the folding process, the intermediate contains hydrogen-bonded structure in the core of the $\beta$F, $\beta$G, $\beta$H, and the major $\alpha$-helix (Kuwata et al. 2001). In hen lysozyme, the fast phase and slow phase of the $\alpha$-domain

both have greater folding rates than those of the $\beta$-domain (Radford et al. 1992). Furthermore, in human fibroblast growth factor, select $\beta$-strands (strands I, IV, IX, and X) form at the same time and constitute the $\beta$-trefoil framework (Samuel et al. 2001). On the other hand, there are cases of other proteins where the formation of hydrogen bonds occurs on a similar time scale. These include the immunoglobulin binding domain of streptococcal protein G (Kuszewski et al. 1994) and bacteriophage $\lambda$ lysozyme (Di Paolo et al. 2010). In our study, as with these latter two proteins, the folding of Fadd-DD also shows cooperative, two-state hydrogen-bond formation. Further, of the 16 evolutionarily conserved residues identified in the death domain superfamily based on a bioinformatics analysis, 10 are well protected and studied in this report (Li et al. 2009). The remaining six cannot be studied as four do not engage in hydrogen bonds, one exchanges too fast, and one cannot be resolved in the HSQC due to peak overlap. Thus, the conserved residues in Fadd-DD are very stable. Overall, the studies presented in this paper with Fadd-DD provide detailed insight into the formation of secondary structure for the all-$\alpha$-helical Greek-key proteins and potentially the all-$\beta$ and mixed $\alpha/\beta$ Greek-key proteins more generally. In the future it would be ideal to find conditions which will enable the long-range hydrogen bond between the indole ring of Trp148 and His160 to be monitored, thus reporting on tertiary structure formation.

These results, combined with consideration of previously published studies that monitored the rate of hydrophobic collapse and the nature of the transition state in Fadd-DD, enable us to further understand the process of secondary and tertiary structure formation in this protein (Supplementary Fig. S2). Our present quenched-flow HX data and previously published stopped-flow fluorescence studies which monitored the hydrophobic collapse (Li et al. 2009) indicate that the two processes occur on similar timescales. Phi-value analysis reveals that helices 1, 2, 4, and 5 are structured in the transition state through specific tertiary interactions (Steward et al. 2009). Thus, it appears that, while all six helices independently and cooperatively form concomitant with the hydrophobic collapse, only helices 1, 2, 4, and 5 interact in the transition state structure, with helices 3 and 6 associating on a later folding timescale.

**Acknowledgments** We express our sincere thanks to Professor Paul Driscoll (University College London) for donation of complementary DNA (cDNA) encoding Fadd-DD, and to John Sonewald (Bio-Logic USA) for technical assistance with the quenched-flow studies. We are grateful to Susan Hatcher (COSMIC Facility, Old Dominion University) for the NMR time. The research was supported by a Jeffress Research Grant (J-889) from the Thomas and Kate Miller Jeffress Memorial Trust and funding from the Old Dominion University Office of Research (to L.H.G.) and an Old Dominion University Graduate Student Fellowship (to H.L.).

## References

Bai Y (2006) Protein folding pathways studied by pulsed- and native-state hydrogen exchange. Chem Rev 106:1757–1768

Bai Y, Milne JS, Mayne L, Englander SW (1993) Primary structure effects on peptide group hydrogen exchange. Proteins 17:75–86

Berglund H, Olerenshaw D, Sankar A, Federwisch M, McDonald NQ, Driscoll PC (2000) The three-dimensional solution structure and dynamic properties of the human FADD death domain. J Mol Biol 302:171–188

Carrington PE, Sandu C, Wei Y, Hill JM, Morisawa G, Huang T, Gavathiotis E, Wei Y, Werner MH (2006) The structure of FADD and its mode of interaction with procaspase-8. Mol Cell 22:599–610

Chen YR, Clark AC (2003) Equilibrium and kinetic folding of an alpha-helical Greek key protein domain: caspase recruitment domain (CARD) of RICK. Biochemistry 42:6120–6310

Chen YR, Clark AC (2004) Kinetic traps in the folding/unfolding of procaspase-1 CARD domain. Protein Sci 13:2196–2206

Chen YR, Clark AC (2006) Substitutions of prolines examine their role in kinetic trap formation of the caspase recruitment domain (CARD) of RICK. Protein Sci 15:395–409

Delaglio F, Grzesiek S, Vuister GW, Zhu G, Pfeifer J, Bax A (1995) NMRPipe: a multidimensional spectral processing system based on UNIX pipes. J Biomol NMR 6:277–293

Di Paolo A, Balbeur D, De Pauw E, Redfield C, Matagne A (2010) Rapid collapse into a molten globule is followed by simple two-State kinetics in the folding of lysozyme from bacteriophage $\lambda$. Biochemistry 49:8646–8657

Dyson HJ, Wright PE (1996) Insights into protein folding from NMR. Annu Rev Phys Chem 47:369–395

Englander SW, Mayne L (1992) Protein folding studied using hydrogen-exchange labeling and two-dimensional NMR. Annu Rev Biophys Biomol Struct 21:243–265

Garcia C, Nishimura C, Cavagnero S, Dyson HJ, Wright PE (2000) Changes in the apomyoglobin folding pathway caused by mutation of the distal histidine residue. Biochemistry 39:11227–11237

Greene LH, Lewis TE, Addou S, Cuff A, Dallman T, Dibley M, Redfern O, Pearl F, Nambudiry R, Reid A, Sillitoe I, Yeats C, Thornton JM, Orengo CA (2007) The CATH domain structure database: new protocols and classification levels give a more comprehensive resource for exploring evolution. Nucleic Acids Res 35:D291–D297

Haglund E, Lind J, Oman T, Ohman A, Mäler L, Oliveberg M (2009) The HD-exchange motions of ribosomal protein S6 are insensitive to reversal of the protein-folding pathway. Proc Natl Acad Sci USA 106:21619–21624

Higman VA, Greene LH (2006) Elucidation of conserved long-range interaction networks in proteins and their significance in determining protein topology. Physica A 368:595–606

Hsieh HC, Kumar TK, Sivaraman T, Yu C (2006) Refolding of a small all beta-sheet protein proceeds with accumulation of kinetic intermediates. Arch Biochem Biophys 447:147–154

Jacobs MD, Fox RO (1994) Staphylococcal nuclease folding intermediate characterized by hydrogen exchange and NMR spectroscopy. Proc Natl Acad Sci USA 91:449–453

Jeong EJ, Bang S, Lee TH, Park YI, Sim WS, Kim KS (1999) The solution structure of FADD death domain. Structural basis of death domain interactions of Fas and FADD. J Biol Chem 274:16337–16342

Jones BE, Matthews CR (1995) Early intermediates in the folding of dihydrofolate reductase from *Escherichia coli* detected by hydrogen exchange and NMR. Protein Sci 4:167–177

Krishna MM, Hoang L, Lin Y, Englander SW (2004) Hydrogen exchange methods to study protein folding. Methods 34:51–64

Kuszewski J, Clore GM, Gronenborn AM (1994) Fast folding of a prototypic polypeptide: the immunoglobulin binding domain of streptococcal protein G. Protein Sci 3:1945–1952

Kuwata K, Shastry R, Cheng H, Hoshino M, Batt CA, Goto Y, Roder H (2001) Structural and kinetic characterization of early folding events in beta-lactoglobulin. Nat Struct Biol 8:151–155

Li H, Wojtaszek JL, Greene LH (2009) Analysis of conservation in the Fas-associated death domain protein and the importance of conserved tryptophans in structure, stability and folding. Biochim Biophys Acta 1794:583–593

Liu C, Gaspar JA, Wong HJ, Meiering EM (2002) Conserved and nonconserved features of the folding pathway of hisactophilin, a beta-trefoil protein. Protein Sci 11:669–679

Lu J, Dahlquist FW (1992) Detection and characterization of an early folding intermediate of T4 lysozyme using pulsed hydrogen exchange and two-dimensional NMR. Biochemistry 31:4749–4756

Milam SL, Nicely NI, Feeney B, Mattos C, Clark AC (2007) Rapid folding and unfolding of Apaf-1 CARD. J Mol Biol 369:290–304

Mullins LS, Pace CN, Raushel FM (1993) Investigation of ribonuclease T1 folding intermediates by hydrogen-deuterium amide exchange-two-dimensional NMR spectroscopy. Biochemistry 32:6152–6156

Nabuurs SM, van Mierlo CP (2010) Interrupted hydrogen/deuterium exchange reveals the stable core of the remarkably helical molten globule of alpha-beta parallel protein flavodoxin. J Biol Chem 285:4165–4172

Nölting B (2006) Protein folding kinetics: biophysical methods, 2nd edn. Springer-Verlag, Berlin Heidelberg, pp 1–4

Park HH, Lo YC, Lin SC, Wang L, Yang JK, Wu H (2007) The death domain superfamily in intracellular signaling of apoptosis and inflammation. Annu Rev Immunol 25:561–586

Parker MJ, Dempsey CE, Lorch M, Clarke AR (1997) Acquisition of native beta-strand topology during the rapid collapse phase of protein folding. Biochemistry 36:13396–13405

Pérez JM, Renisio JG, Prompers JJ, van Platerink CJ, Cambillau C, Darbon H, Frenken LG (2001) Thermal unfolding of a llama antibody fragment: a two-state reversible process. Biochemistry 40:74–83

Primrose WU (1993) Samples preparations. In: Roberts GCK (ed) NMR of macromolecules. Oxford University Press, Oxford, pp 7–34

Radford SE, Dobson CM, Evans PA (1992) The folding of hen lysozyme involves partially structured intermediates and multiple pathways. Nature 358:302–307

Rao PN, Reddy KS, Bhuyan AK (2009) Amyloid fibrillation of human Apaf-1 CARD. Biochemistry 48:7656–7664

Roder H, Elöve GA, Englander SW (1988) Structural characterization of folding intermediates in cytochrome c by H-exchange labelling and proton NMR. Nature 335:700–704

Samuel D, Kumar TK, Balamurugan K, Lin WY, Chin DH, Yu C (2001) Structural events during the refolding of an all beta-sheet protein. J Biol Chem 276:4134–4141

Sasakawa H, Tamura A, Fujimaki S, Taguchi S, Akasaka K (1999) Secondary structures and structural fluctuation in a dimeric protein, Streptomyces subtilisin inhibitor. J Biochem 126:859–865

Schulenburg C, Löw C, Weininger U, Mrestani-Klaus C, Hofmann H, Balbach J, Ulbrich-Hofmann R, Arnold U (2009) The folding pathway of onconase is directed by a conserved intermediate. Biochemistry 48:8449–8457

Steward A, McDowell GS, Clarke J (2009) Topology is the principal determinant in the folding of a complex all-alpha Greek key death domain from human FADD. J Mol Biol 389:425–437

Teilum K, Kragelund BB, Knudsen J, Poulsen FM (2000) Formation of hydrogen bonds precedes the rate-limiting formation of persistent structure in the folding of ACBP. J Mol Biol 301:1307–1314

Udgaonkar JB, Baldwin RL (1988) NMR evidence for an early framework intermediate on the folding pathway of ribonuclease A. Nature 335:694–699

Winn MD, Ballard CC, Cowtan KD, Dodson EJ, Emsley P, Evans PR, Keegan RM, Krissinel EB, Leslie AGW, McCoy A, McNicholas SJ, Murshudov GN, Pannu NS, Potterton EA, Powell HR, Read RJ, Vagin A, Wilson KS (2011) Overview of the *CCP*4 suite and current developments. Acta Cryst D67:235–242